J.Natn.Sci.Foundation Sri Lanka 2023 51 (4): 615 - 628
DOI: http://dx.doi.org/10.4038/jnsfsr.v51i4.11331

RESEARCH ARTICLE

Structural Engineering

A kurtosis-based parameter for classifying elliptical hollow sections under bending

KIU Nanayakkara* **and WPS Dias**
Department of Civil Engineering, Faculty of Engineering, University of Moratuwa, Moratuwa, Sri Lanka.

Submitted: 19 August 2022; Revised: 19 June 2023; Accepted: 28 July 2023

Abstract: A novel section parameter termed *normalized excess kurtosis of a section*, inspired by the same parameter used in probability distributions, is introduced to characterize the rotation capacity of a hollow section under bending. The proposed normalization accounts for variations in yield stress and Young's modulus too. A linear relationship is observed between rotation capacity and the normalized excess kurtosis of circular hollow sections (CHS), rectangular/square hollow sections (RHS) and elliptical/oval hollow sections (EHS), under constant and linearly varying moment conditions, based on experimental and finite element model (FEM) data. It is found that, the rotation capacity variation of hollow sections is better explained by using normalized excess kurtosis than by the conventional section slenderness. The gradient of the above linear relationship varies with the section type and provides an estimate of the rotation capacity of a hollow section with a known shape and aspect ratio. It also provides insights into the section classification of EHS sections, with aspect ratios closer to unity ($0.67 < a/b < 1.5$) being suitable for an equivalent diameter approach and those with aspect ratios further from unity ($a/b < 0.5$ and $a/b > 2.0$) for an equivalent RHS approach. The difference between the moment and rotation capacities of linearly varying moment conditions (3-point bending) and constant moment conditions (4-point bending) is also elucidated.

Keywords: Bending of beams, elliptical hollow sections, kurtosis, rotation capacity, slenderness.

INTRODUCTION

Classification of steel hollow sections

Steel tubular sections are used extensively in the construction industry, from projects such as the Sydney Olympic Stadium to steel framed houses in North America, and in scale from space trusses and frames to wind turbine towers. Along with the rapid rise in usage, research into the same has also picked up during the past couple of decades.

Section classification is central to the design of steel elements (Chen *et al*., 2013). Most of the major design guidelines classify sections into three classes: (i) Class 1, capable of reaching and exceeding full plastic capacity, (ii) Class 2, capable of reaching yield stress at extreme fibres but not full plasticisation, and (iii) Class 3, failing in local collapse before yielding occurs. Slenderness parameters based on section geometry and material yield strength are used for this classification.

However, the existing design codes do not provide guidelines on classification of EHS, although they are now being used extensively in construction. Haque *et al*. (2012) propose an equivalent RHS approach for the

* Corresponding author (isuru_nanayakkara@live.com; https://orcid.org/0000-0003-2630-7724)

classification and design of EHS in axial compression and bending, where EHS sections are transformed to an equivalent RHS and section classification based on RHS slenderness limits. On the other hand, Theofanous *et al*. (2009), Zhu & Wilkinson (2007), Gardner & Chan (2006) and Gardner & Chan (2007) have successfully used an equivalent diameter approach where an EHS is converted to an equivalent CHS.

Furthermore, current codified section classifications use section geometry and material strength as the only input variables, although other parameters have been observed to influence the rotation capacity of a beam and hence the section classification. Sherman (1976) observes that moment gradient and stiffness due to end fixities influence the rotation capacity; and Wang *et al*. (2016) identify aspect ratio, strain hardening and moment gradient as parameters influencing the rotation capacity of RHS. Seif & Schafer (2010) redefine the section slenderness parameter to take web-flange interaction into account.

Classification of sections for plastic frame analysis (*i.e.*, class 1 limit) is based on the available rotation capacity of a beam of uniform section exceeding some pre-defined plastic rotation capacity requirement, the value of which is not clearly intimated to users in current codes of practice. It is the authors' view that a continuous relationship between rotation capacity and section geometry, as opposed to a single point value, allows for better utilization of the capacity available in a beam of a uniform hollow section (*i.e.*, to optimize the section geometry). To maintain the simplicity expected of a design process, it is prudent to relate the rotation capacity to a simple section parameter.

Three primary methods have been used to predict the rotation capacity of beams: (i) empirical methods (*e.g.*, Kato, 1988; Castaldo *et al*., 2017), (ii) analytical solutions, and (iii) soft computing methods (*e.g.*, D'Aniello *et al*., 2015). Empirical methods are hindered by limitations of the data set while analytical solutions face the trade-off between the need for simplicity in design usage and the need to account for complex behaviour. D'Aniello *et al*. (2015) use genetic programming and neural networks to build a predictive model which is both efficient and not influenced by simplifying assumptions; however the model will only be as good as the quality and the breadth of the training set.

The current paper introduces a new section parameter with a view to presenting a simplified relationship with rotation capacity, and to clarify the quandary in classifying EHS as either CHS or RHS. We present a novel section parameter based on the statistical parameter kurtosis. Experimental and finite element model (FEM) data on CHS, EHS/OHS and RHS are studied on the basis of this novel parameter. In particular, we use the parameter to shed light on the dilemma of the section classification for EHS. Finally, we note further insights that can be provided by this novel parameter and the advantages thereof.

Rotation capacity and kurtosis

In mechanics, the zeroth raw moment of area of a cross section gives the area of the section; the first raw moment of area of the cross section as a fraction of the area gives the distance to the centroid; and the second raw moment of area as a fraction of the area yields the well-known definition of radius of gyration.

Moments of area are parameters that appear in both statistics and mechanics. The first order raw moment, second order central moment, third order standardized moment and fourth order standardized moment of a probability distribution function are called the mean, variance, skewness, and kurtosis of the probability distribution, respectively.

Kurtosis is the most misunderstood statistical parameter of the four mentioned above and the hardest to grapple with (DeCarlo, 1997). Kurtosis is an indicator of the shape of a statistical distribution. Kurtosis values for some common distributions are 3.0 for a normal distribution, 1.8 for a uniform distribution of unit variance and 4.2 for a logistic distribution. As DeCarlo (1997) notes, kurtosis should be clearly distinguished from variance and "represents a movement of mass that does not affect the variance." When applied to hollow cross sections, excess kurtosis (see below) acts as a parameter representing the wall thickness of the section, with variance (hence the stress distribution) and area of section being made irrelevant.

Kurtosis of a section (*Kt*) is defined as in equation 1; where I_{x^4} is the fourth moment of area about the x-x axis, which is chosen to coincide with the axis of bending; A is the gross cross-sectional area and r_{xx} is the radius of gyration of the cross-section with reference to the x-x axis (*i.e.*, the axis of bending).

$$Kt = \frac{I_{x^4}}{A\, r_{xx}{}^4} \qquad ...(1)$$

where $I_{x^4} = \int_A y^4\, dA$

The bimodal reference kurtosis (Kt_b) is defined as the kurtosis of the section at an infinitesimally small wall thickness *(t)* (see equation 2). The physical representation of this condition for a hollow section is the concentration of the total area of section at infinitesimally small points at either end along the y-axis; hence a bimodality.

$$Kt_b = \lim_{t \to 0} \frac{I_{x^4}}{A\, r_{xx}{}^4} \quad ...(2)$$

The parameter suggested for the classification of hollow steel sections is $\widehat{Kt}$– *i.e.*, the normalized excess kurtosis of a section (see equation 3); or kurtosis in excess of a pure bimodal distribution, normalized with respect to yield strength (f_y) and modulus of elasticity (E) of the material.

$$\widehat{Kt} = (Kt - Kt_b)\left(\frac{235}{f_y}\right)^{n_1}\left(\frac{E}{210}\right)^{n_2} \quad ...(3)$$

with f_y in MPa and E in GPa.

The reference values of yield strength (f_y) and modulus of elasticity (E) are chosen as 235 MPa and 210 GPa respectively, based on EN 1993-1-1 (2005). The normalization with f_y as denominator and E as numerator follows EN 1993-1-4 (2006) and EN 1993-1-12 (2007). The values n_1 and n_2 are chosen based on the section type (CHS, RHS, or EHS) and loading pattern (constant moment or linearly varying moment).

The concept of excess kurtosis over and above the reference bimodal kurtosis (which is related to thickness concentration at the bimodal points) gives us a parameter related to the wall thickness of the section. In essence, this simplifies the buckling of a hollow section to a single plate buckling problem. It is important to recognize that excess kurtosis has this theoretical basis, and is not merely a parameter that has a fortuitous relationship with rotation capacity. However, the parameter does not take into account the transverse curvature along the wall of the section, which must be accounted for by section shapes and aspect ratios.

Table 1 and Table 2 summarize section slenderness and excess kurtosis values for a series of CHS and RHS. As section slenderness decreases, excess kurtosis increases, as does the rotation capacity. Also, as indicated above, sections with larger thickness have larger excess kurtosis values, provided other section properties are identical. However, a CHS of diameter 150 mm and wall thickness 2 mm gives an excess kurtosis of 365 $\times 10^{-6}$ whereas RHS of section depth 150 mm and same wall thickness gives excess kurtosis values of range around 3,500 to 6,000 $\times$ 10^{-6}. This dependence on shape and aspect ratio will become very evident in the ensuing analysis of data.

Table 1: Excess kurtosis value for typical CHS of different outer diameter and thickness.

Outer diameter (D in mm)	Wall thickness (t in mm)	Section slenderness (D/t)	Excess kurtosis $(Kt - Kt_b\ in\ 10^{-3})$
300	2	150.0	0.09
150	2	75.0	0.37
150	4	37.5	1.50

Table 2: Excess kurtosis value for typical RHS of different section breadth, depth and thickness.

Section breadth (B in mm)	Section height (D in mm)	Wall thickness (t in mm)	Section slenderness		Excess kurtosis $(Kt - Kt_b\ in\ 10^{-3})$
			B/t	D/t	
50	150	1.25	40.0	120.0	3.57
75	150	2.00	37.5	75.0	3.54
50	150	2.00	25.0	75.0	5.94
75	150	4.00	18.8	37.5	8.08

Table 3: Summary of data sources used in the current study

Author(s)	Year	Section type	Experiments / FEM	No. tests
Jiao & Zhao	2004	CHS	4-point bending test (4PB)	12
			Pure bending test	
Guo *et al.*	2013	CHS	4-point bending test	8
Elchalakani *et al.*	2002	CHS	Pure bending test	12
Elchalakani *et al.*	2002	CHS	Pure bending test	9
Kiyamaz	2005	CHS	4-point bending	8
Sedlacek *et al.*	1998	CHS	4-point bending	61
		RHS	3-point bending (only CHS)	18
Sherman	1976	CHS	4-point bending test Cantilever tests	28
Sherman	1986	CHS	Constant moment tests	
			Cantilever tests	
Rasmussen & Hancock	1993	CHS	4-point bending	2
		RHS		
Zheng *et al.*	2016	CHS	4-point bending	8
		RHS		
Theofanous *et al.*	2009	EHS	3-point bending (3PB)	6
			FEM(3PB)	36
Chan & Gardner	2008	EHS	4-point bending	18
			3-point bending	
Wilkinson & Hancock	1998	RHS	4-point bending	44
Korol & Hudoba	1972	RHS	4-point bending	22
Gardner *et al*.	2006	RHS	4-point bending	6
Zhou & Young	2005	RHS	4-point bending	15
Theofanous & Gardner	2010	RHS	3-point bending	8
			FEM (3PB)	36
Huang & Young	2013	RHS	4-point bending	10
			FEM (4PB)	125
Afshan & Gardner	2013	RHS	3-point bending	8
			4-point bending	
Bock *et al.*	2015	RHS	3-point bending	9
			4-point bending	
Theofanous *et al*.	2014	RHS	3-point bending	5
Zhao *et al*.	2015	RHS	4-point bending	5
Zhao *et al*.	2016	RHS	4-point bending	2
Zhao *et al*.	2016	RHS	4-point bending	2
Wang *et al.*	2016	RHS	3-point bending	22
			4-point bending	216
			FEM (3PB/4PB)	
Su *et al.*	2014	RHS	3-point bending	22
			4-point bending	128
			FEM (3PB/4PB)	

MATERIALS AND METHODS

Data collection

Experimental and FEM data were collected from published studies by various authors (see Table 3). The data collected include tests on CHS, RHS, and EHS under both constant and linearly varying moment conditions, and covers a range of geometrical parameters, yield strengths, and material types, as summarized in Table 4.

The geometrical parameters are (i) slenderness ratios – *i.e.*, D/t for CHS, B/t for RHS and ab/t^2 for EHS; and (ii) aspect ratios – *i.e.*, H/B for RHS and a/b for EHS. Here, D is the outer diameter of a CHS; H and B are the height and breadth of an RHS; a and b are the lengths of the major and minor axes of an EHS; and t is the wall thickness (see Figure 1)

.

Table 4: Summary of ranges of geometrical parameters, yield strengths and materials covered in the data set.

Section type	Geometry parameter*	Parameter range	Yield strength (MPa)	Materials
CHS	D/t	6.2–75	190–1,398	Steel (cold formed / hot rolled), stainless steel
RHS	B/t H/B	3.6–61 1.0–6.0	139–813	Steel (cold formed/hot rolled) stainless steel (austenitic, ferritic, duplex, cold worked and annealed), aluminium
EHS	ab/t^2 a/b	83–655 1.0–2.0	317–441	Steel (hot rolled), stainless steel

* The corresponding dimensions are as shown in Figure 1.

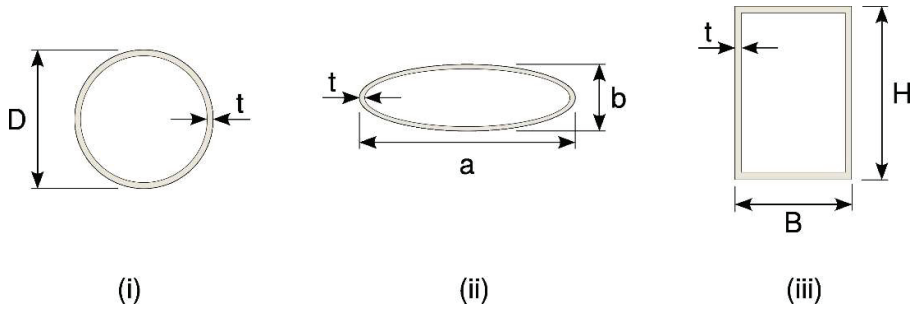

Figure 1: Dimensions of (i) circular hollow sections, (ii) elliptical hollow sections and (iii) rectangular hollow sections.

All the sources of FEM results above have used the ABAQUS software package and the S4R four node doubly curved shell element in their models. Residual stresses were not explicitly included and Theofanous *et al*. (2009) note that the yield strength values used may include this effect. Local geometric imperfections were incorporated in the FE models via the lowest elastic buckling mode shape obtained from linear eigenvalue buckling analysis with appropriate imperfection amplitudes.

The imperfection amplitudes used in the above models are summarized in Table 5. Wang *et al*. (2016), Theofanous *et al*. (2014) and Theofanous & Gardner (2010) have tested multiple imperfection amplitudes before selecting those noted in Table 5.

It was observed that the peak moment is not significantly influenced by the imperfections (*i.e.*, mean errors of about 5% in comparison to experimental results) but the rotation capacity is. The amplitudes selected by Wang *et al*. (2016), Theofanous *et al*. (2009) and Theofanous & Gardner (2010) resulted in mean errors of -6%, + 10% and +12% respectively.

Huang & Young (2019) and Su *et al*. (2014) have not reported corresponding error values. Note that these are not necessarily the smallest average errors observed for rotation capacities in the respective studies, since the imperfection amplitudes had been selected to minimize the errors for the peak moments.

Table 5: Imperfection amplitudes used in FEM models referenced in this study

Author(s)	Imperfection amplitude	Notes
Wang *et al*. (2016)	*t*/50	
Theofanous *et al*. (2009)	*t*/10	
Theofanous & Gardner (2010)	$0.023(\sigma_{0.2}/\sigma_{cr})t$	Dawson and Walker solution as adapted by Theofanous & Gardner (2010)
Huang & Young (2013)	*t*/10	Average measured local imperfection was t/11
Su *et al*. (2014)	0.2 mm	This is the average measured local imperfection

Rotation capacity

Two different ways are used to define the rotation capacity. The two definitions—R_1 and R_2—are as presented in equation 4 and equation 5, where κ_p and κ_u are bending curvatures corresponding to full plastic moment (M_p) and ultimate moment (M_u) while $\vartheta_y, \vartheta_p, \vartheta_{max}$ and ϑ_u are bending rotations corresponding to moment at onset of yield (M_y), full plastic moment (M_p), maximum moment (M_{max}) and the ultimate moment (M_u) as shown in the moment-rotation (curvature) graph in Figure 2.

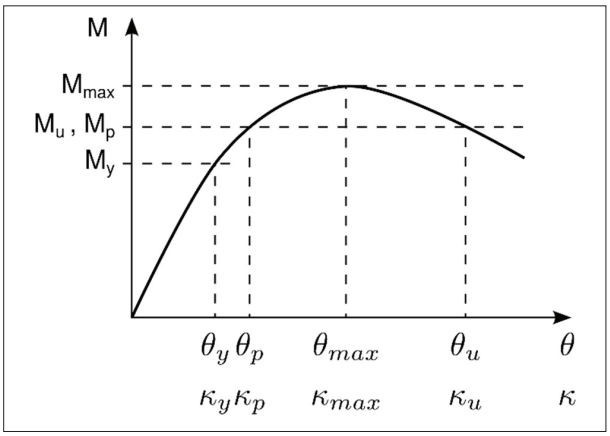

Figure 2: Typical moment - rotation (curvature) plot with reference notation for equations 4 and 5.

$$R_1 = \begin{cases} \frac{\kappa_u}{\kappa_p} - 1\,, & curvature\ measured \\ \frac{\vartheta_u}{\vartheta_p} - 1, & rotation\ measured \end{cases} \quad ...(4)$$

$$R_2 = \frac{\vartheta_{max}}{\vartheta_y} - 1 \quad ..(5)$$

In the equation 4 definition, the choice of curvature or rotation is based on the method of measuring deformation; curvature is primarily used in constant moment tests, and rotation in tests with linearly varying moment.

The equation 5 definition based on Sherman (1976) normalizes the plastic rotation by elastic rotation at first yield (ϑ_y) as opposed to elastic rotation at full plastic moment (ϑ_p) used in the equation 4 definition. Although the numerical values are comparable, the data presented using the equation 5 definition are omitted for the sake of data consistency. Furthermore, the equation 4 definition is superior in that the measurement is of the rotation while maintaining full plastic moment, which is consistent with the definition of Class 2 sections under section classification in EN 1993-1-1 (2005).

RESULTS AND DISCUSSION

Study of experimental and FEM data

The behaviour of rotation capacity against normalized excess kurtosis for CHS, RHS, and EHS under linearly varying moment was studied (CHS - Figure 3, RHS - Figure 4, EHS - Figure 5). Data points considered are from experimental data, complemented by FEM data where available.

Only experimental data were available for CHS while both experimental and FEM data were available for the study of RHS and EHS. Some experimental data were available from constant moment tests on EHS; however only four valid data points were available for the trendline and this was deemed too few for any reasonably conclusive study. As such this study is focused on linearly varying moment conditions. However, the authors would

anticipate a similar behaviour under the constant moment condition, as explained later.

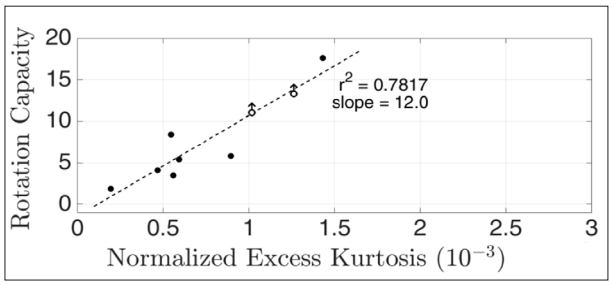

Figure 3: Rotation capacity vs normalized excess kurtosis of experimental data from linearly varying moment tests on CHS. The dashed line indicates the trendline. Markers with arrows indicate that tests stopped prematurely (*i.e.*, full rotation capacity not achieved).

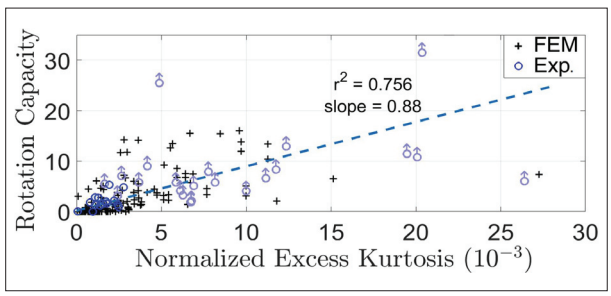

Figure 4: Rotation capacity vs normalized excess kurtosis of experimental and FEM data from linearly varying moment tests on RHS. Dashed line indicates the linear trend of the combined data. Markers with arrows indicate tests stopped prematurely (*i.e.*, full rotation capacity not achieved).

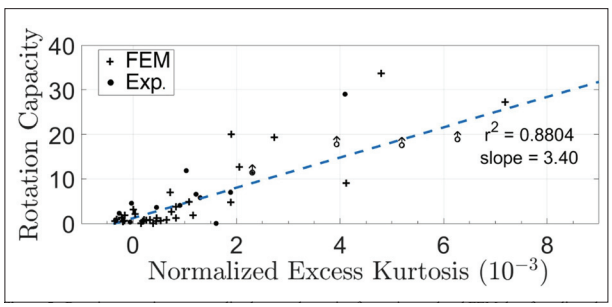

Figure 5: Rotation capacity vs normalized excess kurtosis of experimental and FEM data from linearly varying moment tests on EHS. Dashed line indicates the linear trend of the combined data. Markers with arrows indicate tests stopped prematurely (*i.e.*, full rotation capacity not achieved).

For CHS, $n_1 = n_2 = 2.2$ was used and for RHS, $n_1 = n_2 = 1.0$. The value for CHS is based on the semi-empirical equation derived in the Appendix – under the selected value the rotation capacity vs normalized excess kurtosis relationship is insensitive to yield strength and modulus of elasticity. A similar semi-empirical equation for RHS gives a variable function for n_1 and n_2, but a constant value of unity is chosen for simplicity. This value gives the highest coefficient of correlation for the rotation capacity versus normalized excess kurtosis linear regression line. For EHS, $n_1 = n_2 = 2.2$ was borrowed from CHS since the semi-empirical equation cannot be derived, with no reliable base curve being available for EHS in the current literature. It is noted that using $n_1 = n_2 = 1.0$ —the value used for RHS—would result in the same general conclusions, albeit different slopes for excess kurtosis-rotation capacity relationship of EHS.

The linear trendline was plotted using the data points, subject to the data qualification processes described in the following paragraphs. A robust least-squares fitting process with bisquare weights was used to minimize the effect of outliers.

In both the experimental and FEM data sets there were several tests in which the sections did not reach the plastic moment capacity, and consequently a rotation capacity of zero was recorded. At the other extreme there were points where the full rotation capacity was not achieved due to limitations in the experimental set up: *e.g.*, limits on loading and/or deflection measurements and/or limitations on the loading apparatus. The latter values are noted in the graphs with an upward arrow marker to indicate that the actual rotation capacities would be higher than the recorded value. Both these types of data are ignored in trendlines.

It was also observed that rotation capacities (for both experimental and FEM data) start to drop from the linear trend at very high $\widehat{Kt}$. These rotations could be low due to two reasons. At very high $\widehat{Kt}$, very high rotation capacities are expected. This in turn means that deflections may no longer satisfy small deformation assumptions, thus invalidating curvature calculations. Furthermore, at higher deflections the ductility requirement of the material may have been exceeded, possibly leading to failure of material by reaching the ultimate strain. As such the data points beyond $\widehat{Kt} = 3 \times 10^{-3}$ in CHS and 10×10^{-3} in RHS are ignored in the trendlines. In any case these sections would be having rotation capacities well beyond the rotation capacity demands for common structural engineering applications, therefore having no impact on the usage of the simple linear relationship for the purpose of section classification.

For both RHS and EHS (Figures 4 and 5 respectively), experimental data were observed to be consistent with the FEM data even though the data came from multiple sources. FEM data were not available for comparison in CHS data.

For all three section types studied, a monotonic trend was observed, with rotation capacity increasing as normalized excess kurtosis increases. At the same time, a considerable scatter is observed in the data.

A primary reason for the scatter observed in the data is the geometrical imperfections in the members. The FE model by Theofanous *et al*. (2009) shows that omitting imperfections in the model would result in the overestimation of rotation capacity by 38% on average (compared to experimental results used for the verification of the corresponding FE model); and using the measured imperfections would underestimate the rotation capacity by 8%. Furthermore, individual errors in the range of 67% were observed.

Still higher discrepancies were observed in experimental results even where the same nominal section of the same material was tested under the same loading systems. Guo *et al.* (2013) observed rotation capacities of 1.2, 1.6 and 3.2 for three CHS specimens of outer diameter 300 mm, thickness 2 mm and yield strength 190 MPa; and Sherman (1986) observed rotation capacities of 5.9 and 8 for two CHS specimens of outer diameter 458 mm, thickness 10.29 mm and yield strength 341 MPa. Similarly, Theofanous *et al*. (2009) observed rotation capacities of 2.28 and 4.59 for EHS sections of nominal major and minor axes 121 mm and 76 mm, thickness 2 mm and yield strength 380 MPa.

A significant number of such discrepancies were observed in RHS sections as well. Wilkinson and Hancock (1998) observed rotation capacities of 5.9 and 0 (failure before reaching plastic moment capacity) for two RHS specimens of breadth 25 mm, depth 75 mm, thickness 2 mm and yield strength 467 MPa. They further report rotation capacities of 1.1, 1.2, 1.4 and 2.2 for a series of RHS specimens of breadth 50 mm, depth 150 mm, thickness 2.3 mm and yield strength 456 MPa. Zheng *et al*. (2016) report rotation capacities of 5.4 and >10.7 (no failure at termination of experiment) for a series of square hollow section (SHS) specimens of breadth and depth of 100 mm, thickness 3 mm and yield strength 408 MPa. The above are only a sample of individual data points that show the inherent scatter of the data and they are most likely due to the geometrical imperfections in the beams tested.

Another minor reason for the scatter is the experimental procedures followed. The data are collected from experiments conducted with varying facilities, equipment, procedures, and personnel. As such we should give due recognition to the fact that there is the possibility of inconsistencies between some data sets. Attempts to account for all minor discrepancies will lose the generality of possible conclusions. As mentioned earlier a robust least square fitting with bisquare weights was used to allow for these outliers.

The same data set was considered to study the relationship between the rotation capacity and the section slenderness as defined in EN 1993-1-1 (2005). We have compared the corresponding R-squared values under a linear regression with bisquare robust fitting (see Table 6) and found that excess kurtosis fits better to a linear relationship with rotation capacity. Note that rotation capacity increases monotonically with excess kurtosis while decreasing monotonically with section slenderness.

Since there are two section slenderness parameters for RHS – for the web and flange – the critical slenderness was considered. The critical slenderness was determined based on the section slenderness as a fraction of the corresponding upper class 2 limit on section slenderness, as given in EN 1993-1-1 (2005) – *i.e.*, 83ε and 38ε for web and flange respectively.

Table 6: Comparison of R-squared values for (i) rotation capacity vs section slenderness and (ii) rotation capacity vs excess kurtosis relationships, for linear regression with bisquare robust fitting

	Rotation capacity against	
	Section slenderness	Excess kurtosis
CHS (experimental)	0.397	0.782
RHS (experimental and FEM)	0.613	0.756

Table 7: Gradients of rotation capacity vs normalized excessive kurtosis for major axis bending of RHS under varying D/B ranges.

Nominal *D/B*	*D/B* range	Number of data points	Gradient	r^2
0.714	0.714	7	2.16	0.6312
1.00	0.8–1.0	55	2.34	0.7331
1.50	1.25–1.5	13	1.94	0.8691
2.00	2.0	30	1.27	0.9546
2.50	2.4–2.6	21	1.16	0.9151

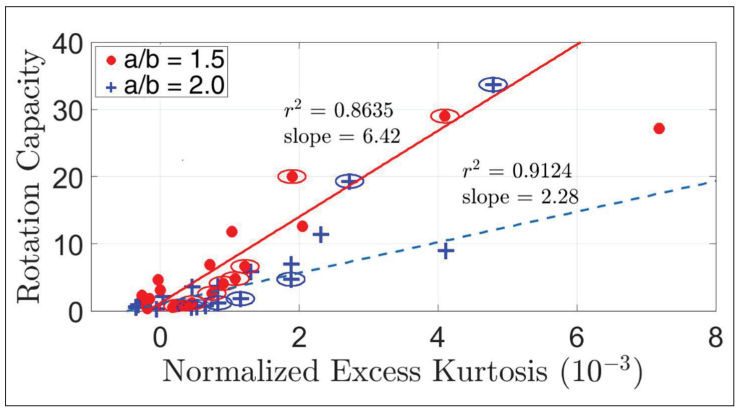

Figure 6: Rotation capacity of EHS under linearly varying moment condition, from experimental and FEM data, differentiated based on aspect ratio. A circle around data point marker indicates bending about major axis.

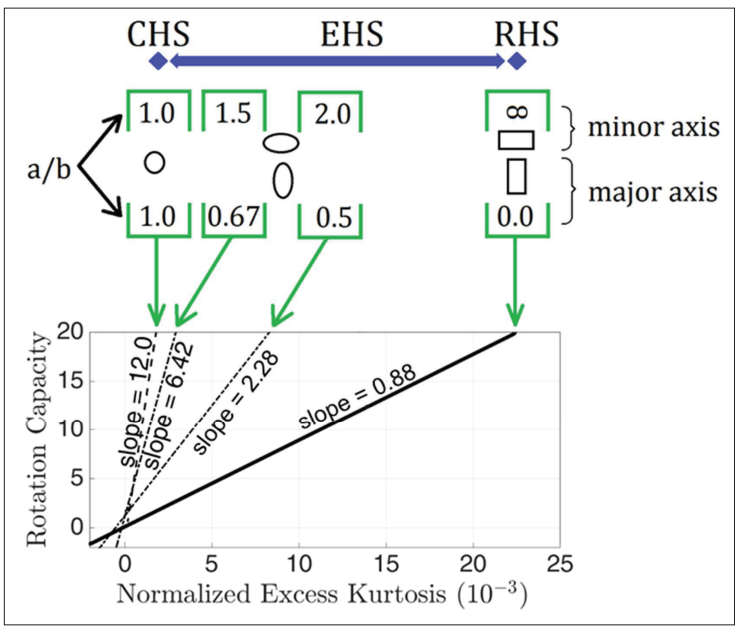

Figure 7: Trend lines observed from data (both experimental and FEM) for CHS, EHS and RHS under linearly varying moment conditions.

Effect of aspect ratio and axis of bending on rotation capacity

Examination of data for RHS show an ordering of the gradient when grouped based on the aspect ratio (*D/B*) (see Table 7). Under major axis bending RHS sections show decreasing gradient with increasing aspect ratio. (from *D/B* = 1.0 to 2.5). There is also a slight decrease in gradient from *D/B* = 1.0 to 0.714, indicating that gradient decreases as *D/B* moves away (in either direction) from unity. This is reflected in the EHS data below too.

Experimental and FEM data of EHS display a much more obvious ordering and significant change in gradient when grouped based on aspect ratio, with a change of gradient from 2.28 to 6.42 in EHS as compared to 1.27 to 1.94 in RHS, for a change in aspect ratio from 2.0 to 1.5. Furthermore, there is no discernible effect due to axis of bending (Figure 6). Note that Figure 6 includes both major and minor axis bending, with symbols enclosed in a loop indicating bending about major axis.

The above collation of data—both experimental and FEM—on CHS, RHS and EHS, based on multiple aspect ratios, leads to an interesting observation, where in essence EHS can be thought of as an intermediate state between RHS and CHS – see Figure 7 for the linearly varying moment condition. Note that the RHS slope is based on all the data in Figure 4, but disaggregated in Table 7. Because slopes are obtained by bisquare fitting the overall RHS slope in Figures 4 and 7 does not fall within the slopes in Table 7, but is similar in magnitude.

The above observations (clearly visible in Figure 7) counter the claims for using a single equivalent RHS or equivalent CHS approach for the classification of EHS, and shows that the EHS behaviour varies between CHS and RHS as the aspect ratio changes; an aspect ratio closer to 1 indicates more CHS-like behaviour while an aspect ratio closer to 0.0 or infinity (or practically < 0.5 or > 2.0) indicates more RHS like behaviour. Interestingly, most of the data used by Haque *et al*. (2012) to validate the equivalent RHS behaviour are of aspect ratio of 2.0 (or 0.5).

It is obvious that minor and major axis lengths (*a* and *b*) for an equivalent CHS are equal to unity (1.0), but this is less clear for an equivalent RHS. Note that the values of aspect ratio act as indicators of transverse curvature along the wall of the hollow section. As such we can consider an RHS having a very large breadth to be having an infinitely long horizontal axis – see Figure 1(iii), where the top and bottom flanges will become virtually a single plate with zero curvature. By a similar argument the RHS having a very large height can be considered as having an infinitely long vertical axis and webs once again with zero curvature.

We have noted early on that excess kurtosis does not take into account the effect of geometric transverse curvature of the wall of the hollow section. It is now evident that aspect ratio based on minor and major axis length accounts for the transverse curvature along the wall of the hollow section. Circular sections have the greatest curvatures followed by elliptical sections, with that of rectangular sections approaching zero. As curvatures decrease the slopes in Figure 7 also decrease. Based on Figure 7 we can say that EHS with aspect ratios closer to unity ($0.67 < a/b < 1.5$) should be classified based on an equivalent diameter approach, and those with aspect ratios further from unity ($a/b < 0.5$ and $a/b > 2.0$) based on an equivalent RHS approach. The actual normalized excess kurtosis limits for classification of hollow sections (from CHS to RHS, through EHS) can be based on Figure 7. For this, an appropriate confidence line (where, say 95%, of all values lie above the line) can be used, instead of the average trend line used here for identifying the distinctions across the types of sections.

We only present and discuss the behaviour under the linearly varying moment condition due to limited availability of data – EHS data for constant moment conditions were available for only one aspect ratio. We have observed however similar patterns with the constant moment condition for CHS and RHS, with constant moment conditions giving a higher rotation capacity than the linearly varying moment condition, for a given normalized excess kurtosis.

Excess kurtosis vs slenderness ratio

Slenderness is the currently used parameter in design codes to relate rotation capacity with section geometry. This relationship is such that if the section slenderness is smaller than a given value then the rotation capacity is sufficient for a plastic analysis to be carried out. The value of this 'sufficient rotation capacity' is not clear, but suggested values can be inferred from Korol & Hudoba (1972).

The slenderness parameter and the limiting slenderness value are different for different section types – *e.g.*, *c/t* for each plate in RHS with $(33\sqrt{235/f_y})$ as the limit for parts in compression only and *D/t* for CHS with $(50 \times 235/f_y)$ as the limit (EN 1993-1-1: 2005). Furthermore, Jiao & Zhao (2004) note that, even

after normalizing for material strength, the relevant slenderness limit for very high strength steel (f_y = 1350 MPa) is different from that for normal strength steel (f_y = 350–450 MPa).

Although both slenderness ratio and excess kurtosis can be used to determine a continuous relationship between rotation capacity and section geometry, the latter is superior as it (i) uses a common equation for CHS, RHS and EHS sections and (ii) gives the same rotation capacity value regardless of the material strength (*e.g.*, valid for both very high strength and normal strength steel).

The rotation capacity of sections, within the range of geometry in commonly used CHS and RHS sections, is influenced by local buckling. As such, using section slenderness to relate to rotation capacity is intuitive (since we use member slenderness to relate to overall buckling). However, although not immediately obvious, the excess kurtosis of a section is a measure of the wall thickness of hollow sections, as stated early on. Use of excess kurtosis simplifies the rotation capacity problem to a plate buckling problem, while the different slopes in Figure 7 account for the curvature of the plate in the transverse direction.

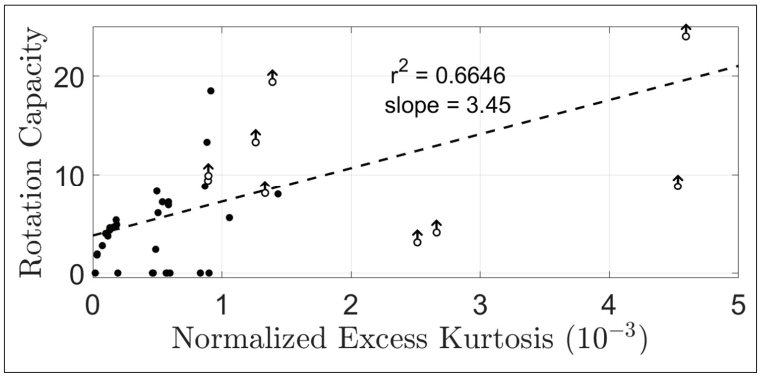

Figure 8: Rotation capacity vs normalized excess kurtosis of experimental data from constant moment tests on CHS. Markers with arrows indicate tests stopped prematurely (*i.e.*, full rotation capacity not achieved).

Effect of loading system

We have so far presented data under the varying moment condition. Figure 8 presents the behaviour of rotation capacity against normalized excess kurtosis under the constant moment condition. Experimental data for CHS indicate a higher rotation capacity under linearly varying moment (Figure 3) than under constant moment conditions (Figure 8).

Most of our data and analysis are for the varying moment condition (*e.g.*, Figure 3 for CHS). Figure 8 however, allows this to be compared with the behaviour under a constant moment condition. The trendlines from the experimental data for CHS indicate a higher rotation capacity under linearly varying moment (Figure 3) than under constant moment conditions (Figure 8), at higher normalized excess Kurtosis values (say > $1x10^{-3}$), and vice versa at lower values.

CONCLUSION

In this study, a novel section parameter termed normalized excess kurtosis of a hollow section has been derived. It is inspired by a parameter of similar name in the field of statistics and is a measure of the wall thickness of hollow sections. It demonstrates a linear relationship with the rotation capacity of the section, hence giving a simple method to estimate rotation capacity of circular hollow sections (CHS), rectangular/square hollow sections (RHS) and elliptical/oval hollow sections (EHS).

Given a CHS, an RHS, and an EHS having the same normalized excess kurtosis, the CHS, which has the highest transverse curvature (*i.e.*, a section aspect ratio of 1.0) will have the largest rotation capacity; RHS, with the smallest transverse curvature (*i.e.*, having an aspect ratio tending to infinity) the smallest rotation capacity; and EHS, with an intermediate curvature, a rotation capacity between that of the CHS and the RHS.

It is observed that EHS presents a CHS–like behaviour at aspect ratios (a/b) closer to 1.0 and an RHS-like behaviour at high (say >2.0) or low (say < 0.5) aspect ratios. Thus, the equivalent RHS or equivalent CHS approaches can be appropriately applied to EHS, for use in plastic analysis.

Acknowledgements

The authors sincerely acknowledge the assistance provided by Prof. Ben Young, Dr Marios Theofanous, Dr Mei-Ni Su, and Dr Michaela Gkantou in sharing their FEM data sets; and Prof. Leroy Gardner, Dr Mohamed Elchalakani, and Dr Fulop Ludovic for the additional data and clarifications on data provided. Comments and suggestions from Prof. David Nethercot are especially appreciated.

REFERENCES

Afshan S. & Gardner L. (2013). Experimental study of cold-formed ferritic stainless steel hollow sections. *Journal of Structural Engineering* **139**(5): 717–728. DOI: https://doi.org/10.1061/(ASCE)ST.1943-541X.0000580

Bock I., Arrayago I. & Real E. (2015). Experiments on cold-formed ferritic stainless steel slender sections. *Journal of Constructional Steel Research* **109**: 13–23. DOI: https://doi.org/10.1016/j.jcsr.2015.02.005

Castaldo P., Nastri E. & Piluso V. (2017). Ultimate behaviour of RHS temper T6 aluminium alloy beams subjected to non-uniform bending: Parametric analysis. *Thin-Walled Structures* **115**: 129–141. DOI: https://doi.org/10.1016/j.tws.2017.02.006

Chan T. & Gardner L. (2008). Bending strength of hot-rolled elliptical hollow sections. *Journal of Constructional Steel Research* **64**: 971–986. DOI: https://doi.org/10.1016/j.jcsr.2007.11.001

Chen Y., Cheng X. & Nethercot D.A. (2013). An overview study on cross-section classification of steel H-sections. *Journal of Constructional Steel Research* **80**: 386–393. DOI: https://doi.org/10.1016/j.jcsr.2012.10.006

D'Aniello M., Güneyisi E.M., Landolfo R. & Mermerdaş K. (2015). Predictive models of the flexural overstrength factor for steel thin-walled circular hollow section beams. *Thin-Walled Structures* **94**: 67–78. DOI: https://doi.org/10.1016/j.tws.2015.03.020

DeCarlo L.T. (1997). On the meaning and use of kurtosis. *Psychological Methods* **2**(3): 292–307. DOI: https://doi.org/10.1037/1082-989X.2.3.292

Elchalakani M. (2014). A closed formed solution for elastic buckling of thin-walled unstiffned circular cylinders in pure flexure. *Thin-Walled Structures* **80**: 120–129. DOI: https://doi.org/10.1016/j.tws.2014.03.002

Elchalakani M., Zhao X.L. & Grzebieta R. (2002a). Bending tests to determine slenderness limits for cold-formed circular hollow sections. *Journal of Constructional Steel Research* **58**: 1407–1430. DOI: https://doi.org/10.1016/S0143-974X(01)00106-7

Elchalakani M., Zhao X.L. & Grzebieta R. (2002b). Plastic slenderness limits for cold-formed circular hollow sections. *Australian Journal of Structural Engineering* **3**(3): 127–139. DOI: https://doi.org/10.1080/13287982.2002.11464900

EN1993-1-1:2005. Eurocode 3: Design of Steel Structures: Part 1-1: General Rules and Rules for Buildings. European Committee for Standardization, Brussels.

EN 1993-1-4:2006. Eurocode 3: Design of steel structures: Part 1-4: General rules - Supplementary rules for stainless steels. European Committee for Standardization, Brussels.

EN 1993-1-12:2007. Eurocode 3: Design of steel structures: Part 1-12: Additional rules for the extension of EN 1993 up to steel grades S 700. European Committee for Standardization, Brussels.

Gardner L. & Chan T. (2006). Cross section classification of elliptical hollow sections. In: *Proceedings of the 11th International Symposium on Tubular Structures*. Québec City, Canada.

Gardner L. & Chan T. (2007). Cross-section classification of elliptical hollow sections. *Steel and Composite Structures* **7**(3): 185–200.

Gardner L., Talja A. & Baddoo N. (2006). Structural design of high-strength austenitic stainless steel. *Thin-Walled Structures* **44**: 517–528. DOI: https://doi.org/10.1016/j.tws.2006.04.014

Guo L., Yang S. & Jiao H. (2013). Behaviour of thin-walled circular hollow section tubes subjected to bending. *Thin-Walled Structures* **73**: 281–289. DOI: https://doi.org/10.1016/j.tws.2013.08.014

Haque T., Packer J.A. & Zhao X.L. (2012). Equivalent RHS approach for the design of EHS in axial compression or bending. *Advances in Structural Engineering* **15**(1): 107–120. DOI: https://doi.org/10.1260/1369-4332.15.1.107

Huang Y. & Young B. (2013). Experimental and numerical investigation of cold-formed lean duplex stainless steel flexural members. *Thin-Walled Structures* **73**: 216–228. DOI: https://doi.org/10.1016/j.tws.2013.07.019

Jiao H. & Zhao X.L. (2004). Section slenderness limits of very high strength circular steel tubes in bending. *Thin-Walled Structures* **42**: 1257–1271. DOI: https://doi.org/10.1016/j.tws.2004.03.020

Kato B. (1988). Rotation capacity of steel members subject to local buckling. In: *Proceedings of Ninth World Conference on Earthquake Engineering*. Tokyo – Kyoto, Japan.

Kiyamaz G. (2005). Strength and stability criteria for thin-walled stainless steel circular hollow section members under bending. *Thin-Walled Structures* **43**: 1534–1549. DOI: https://doi.org/10.1016/j.tws.2005.06.006

Korol R.M. & Hudoba J. (1972). Plastic behaviour of hollow

structural sections. *Journal of The Structural Division* **98**: 1007–1023.
DOI: https://doi.org/10.1061/JSDEAG.0003221

Rasmussen K. & Hancock G. (1993). Design of cold-formed stainless steel tubular members: II - beams. *Journal of Structural Engineering* **119**(8): 2368–2386.
DOI: https://doi.org/10.1061/(ASCE)0733-9445(1993)119:8(2368)

Sedlacek G. *et al*. (1998). *Investigation of the Rotation Behaviour of Hollow Section Beams*. Office for Official Publications of the European Communities, Luxembourg.

Seif M. & Schafer B.W. (2010). Local buckling of structural steel shapes. *Journal of Constructional Steel Research* **66**: 1232–1247.
DOI: https://doi.org/10.1016/j.jcsr.2010.03.015

Sherman D.R. (1976). Tests of circular steel tubes in bending. *Journal of the Structural Division* **95**: 2181–2195.
DOI: https://doi.org/10.1061/JSDEAG.0004478

Sherman D. (1986). Inelastic flexural buckling of cylinders. In: *International Conference on Steel Structures: Recent Research Advances and their Application to Design*. Amsterdam, Netherlands.

Su M.N., Young B. & Gardner L. (2014). Deformation-based design of aluminium alloy beams. *Engineering Structures* **80**: 339–349.
DOI: https://doi.org/10.1016/j.engstruct.2014.08.034

Theofanous M., Chan T. & Gardner L. (2009). Flexural behaviour of stainless steel oval hollow sections. *Thin-Walled Structures* **47**: 776–787.
DOI: https://doi.org/10.1016/j.tws.2009.01.001

Theofanous M. & Gardner L. (2010). Experimental and numerical studies of lean duplex stainless steel beams. *Journal of Constructional Steel Research* **66**: 816–825.
DOI: https://doi.org/10.1016/j.jcsr.2010.01.012

Theofanous M., Saliba N., Zhao O. & Gardner L. (2014). Ultimate response of stainless steel continuous beams. *Thin-Walled Structures* **83**: 115–127.
DOI: https://doi.org/10.1016/j.tws.2014.01.019

Wang J., Afshan S., Gkantou M., Theofanous M., Baniotopoulos C. & Gardner L. (2016). Flexural behaviour of hot-finished high strength steel square and rectangular hollow sections. *Journal of Constructional Steel Research* **121**: 97–109.
DOI: https://doi.org/10.1016/j.jcsr.2016.01.017

Wilkinson T. & Hancock G.J. (1998). Compact or Class 1 limits for rectangular hollow sections in bending. In: *Tubulur Structures* VIII, *Proceedings, 8th International Symposium on Tubular Structures*, Singapore, pp 409–416.

Zhao O., Gardner L. & Young B. (2016). Buckling of ferritic stainless steel members under combined axial compression and bending. *Journal of Constructional Steel Research* **117**: 35–48.
DOI: https://doi.org/10.1016/j.jcsr.2015.10.003

Zhao O., Rossi B., Gardner L. & Young B. (2015). Behaviour of structural stainless steel cross-sections under combined loading - Part I: Experimental study. *Engineering Structures* **89**: 236–246.
DOI: https://doi.org/10.1016/j.engstruct.2014.11.014

Zhao O., Rossi B., Gardner L. & Young B. (2016). Experimental and numerical studies of ferritic stainless steel tubular cross sections under combined compression and bending. *Journal of Structural Engineering* **142**(2): 04015110.
DOI: https://doi.org/10.1061/(ASCE)ST.1943-541X.0001366

Zheng B., Shu G., Xin L., Yang R. & Jiang Q. (2016). Study on the bending capacity of cold-formed stainless steel hollow sections. *Structures* **8**: 63–74.
DOI: https://doi.org/10.1016/j.istruc.2016.08.007

Zhou F. & Young B. (2005). Tests of cold-formed stainless steel tubular flexural members. *Thin-Walled Structures* **43**: 1325–1337.
DOI: https://doi.org/10.1016/j.tws.2005.06.005

Zhu Y. & Wilkinson T. (2007). *Finite Element Analysis of Structural Steel Elliptical Hollow Sections in Compression*. School of Civil Engineering, The University of Sydney, Sydney, Australia.

APPENDIX

Consider a beam of uniform stiffness under 3 point bending. We shall calculate the deflection at mid span of the beam under elastic response (Δ_{el}) from Mohr's second theorem based on the M/EI plot (see Figure A.1), where M is the bending moment, E is the modulus of elasticity, I is the second moment of area and L is the span length.

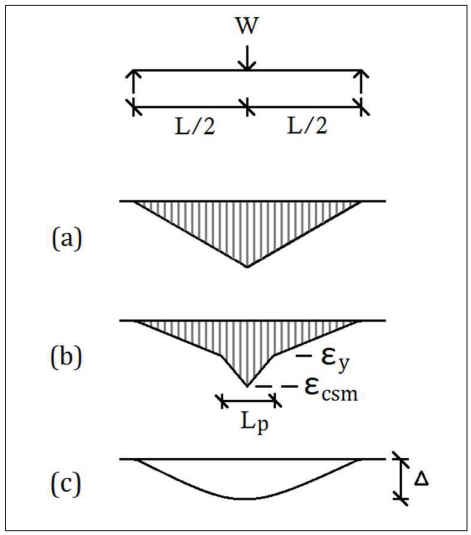

Figure A.1: (a) M/EI diagram within elastic material response, (b) strain plot beyond elastic limit, and (c) deflection pattern, under 3 point bending resulting in linearly varying moment in the mid-span.

Similarly, the deflection at mid span beyond the elastic limit (Δ) is calculated using the strain plot under linearly varying moment conditions, where $\kappa(s)$ is the bending curvature at a distance s from the point of reference, β is the strain capacity, $\bar{\beta}$ is the strain capacity adjusted for linearly varying moment, ε_y is yield strain, S_F is the shape factor, and ρ is the moment ratio.

$$\Delta = \int_0^L \kappa(s)(L-s)ds = \bar{\beta}\varepsilon_y \frac{L^2}{12d}; \quad \text{...(S1)}$$

where $\bar{\beta} = \left[\left(1+\frac{1}{\rho S_F}\right) + \beta\left(\frac{(\rho S_F - 1)(2\rho S_F + 1)}{(\rho S_F)^2}\right)\right]$

$$\rho = \frac{M_{csm}}{M_p} = \left[1 + \frac{E_{sh}}{E}\frac{1}{S_F}(\beta - 1) - \left(1 - \frac{1}{S_F}\right)\frac{1}{\beta^2}\right]$$

$$S_F = \frac{M_p}{M_y}$$

The base curve relates the strain capacity to section properties and Buchanan *et al*. (2016) present one for circular hollow sections, where λ is the section slenderness, f_{crt} the elastic buckling strength, ν the Poisson ratio and ε_{csm} the limiting strain under the continuous strength method.

$$\lambda = \sqrt{\frac{f_y}{f_{crt}}} = \sqrt{\frac{f_y\sqrt{3(1-\nu^2)}}{E}\frac{D}{t}} \quad \text{...(S2)}$$

$$\beta = \frac{\varepsilon_{csm}}{\varepsilon_y} = \frac{4.44\times10^{-3}}{\lambda^{4.5}}; for\ \lambda \leq 0.3 \quad \text{...(S3)}$$

The mid span deflection is related to bending curvature (κ) using equation (S4) assuming a uniform curvature along the beam. However this is strictly applicable only to a constant moment condition. Note that this assumption overstates the rotation under linearly varying moment conditions, where the rotation is localised due to the moment gradient.

$$\kappa = \frac{1}{R} = \frac{8\Delta}{4\Delta^2 + L^2} \quad \text{...(S4)}$$

The resulting elastic curvature at full plastic moment (κ_p) and at maximum moment (κ_{max}) can be formed as;

$$\kappa_p = \frac{24M_pEI}{(M_pL)^2 + (6EI)^2} \quad \text{...(S5)}$$

$$\kappa_{max} = \frac{24\bar{\beta}\varepsilon_y d}{(\bar{\beta}\varepsilon_y L)^2 + (6d)^2} \quad \text{(S6)}$$

The resulting rotation capacity is;

$$R_3 = \frac{\kappa_{max}}{\kappa_p} - 1 = \frac{2\bar{\beta}}{S_F}\frac{\left[(S_F\varepsilon_y L)^2 + (3d)^2\right]}{\left[(\bar{\beta}\varepsilon_y L)^2 + (6d)^2\right]} - 1 \quad \text{...(S7)}$$

Note that the equation S7 gives rotation capacity only up to the maximum moment (see Figure A.1); the post buckling behaviour is not accounted for. Such behaviour will depend on the collapse mechanisms formed and this in turn would depend on the section type.

APPENDIX REFERENCES

Buchanan C., Gardner L. & Liew A. (2016). The continuous strength method for the design of circular hollow sections. *Journal of Constructional Steel Research* **118**: 207–216. DOI: https://doi.org/10.1016/j.jcsr.2015.11.006